

Journal of Nuclear Science and Technology

ISSN: 0022-3131 (Print) 1881-1248 (Online) Journal homepage: www.tandfonline.com/journals/tnst20

Modeling of distribution parameters for upward steam-water boiling flows in subchannels of a vertical rod bundle

Tetsuhiro Ozaki & Takashi Hibiki

To cite this article: Tetsuhiro Ozaki & Takashi Hibiki (2023) Modeling of distribution parameters for upward steam-water boiling flows in subchannels of a vertical rod bundle, Journal of Nuclear Science and Technology, 60:12, 1481-1499, DOI: 10.1080/00223131.2023.2225519

To link to this article: https://doi.org/10.1080/00223131.2023.2225519

Published online: 19 Jul 2023.

Submit your article to this journal

Article views: 303

View related articles

View Crossmark data

Citing articles: 11 View citing articles

Full Terms & Conditions of access and use can be found at
https://www.tandfonline.com/action/journalInformation?journalCode=tnst20

JOURNAL OF NUCLEAR SCIENCE AND TECHNOLOGY
2023, VOL. 60, NO. 12, 1481–1499
https://doi.org/10.1080/00223131.2023.2225519

Check for updates

Modeling of distribution parameters for upward steam-water boiling flows in subchannels of a vertical rod bundle

Tetsuhiro Ozaki[a] and Takashi Hibiki[b]

[a]TEPCO Systems Corporation, Shibusawa City Place Eitai, Tokyo Japan; [b]Department of Mechanical Engineering, City University of Hong Kong, Kowloon Tong, Hong Kong, SAR

ABSTRACT

In simulations of two-phase flow behavior in nuclear reactors, subchannel analysis codes are often used to evaluate the void fraction within a BWR fuel bundle in detail. When solving the momentum conservation equation averaged over a subchannel cross-section for upward two-phase flows, the distribution parameter is required to consider the void fraction and velocity distributions in the subchannel cross-section. In this paper, constitutive equations were developed for the distribution parameters for dispersed two-phase flows applicable to the inner, edge, and corner subchannels, which are typical subchannels in a fuel bundle. The distribution parameters could be calculated by giving the void fraction and the velocity distribution. Therefore, the distribution parameters were evaluated and modeled as a function of the geometrical parameters by assuming the void fraction and velocity distributions with bulk and subcooled boiling for each subchannel type. The developed constitutive equations were evaluated by comparing them with the distribution parameters estimated based on the NUPEC rod bundle void fraction test data. The developed distribution parameter model was implemented into the subchannel analysis code NASCA and compared with the measured cross-sectional average void fraction of the NUPEC rod bundle void fraction test data. In comparison with the original NASCA code, which assumed the distribution parameter to be unity, the improved NASCA with the distribution parameter model decreased the mean error of the measured cross-sectional average void fraction to less than half of the result of the original NASCA code, both in absolute and relative differences.

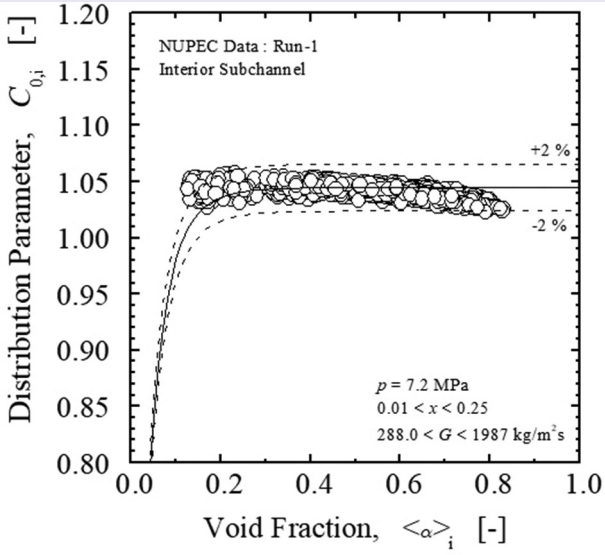

ARTICLE HISTORY
Received 17 October 2022
Accepted 4 April 2023

KEYWORDS
Subchannel analysis; distribution parameter; drift-flux model; rod bundle; reactor core analysis

1. Introduction

Boiling water two-phase flow has been utilized in engineering facilities as a heat transfer system because of its excellent heat transfer characteristics. In LWRs, the heat generated from fissile materials such as uranium is effectively transferred to the coolant, and the generated steam rotates a turbine to extract electrical energy. In a BWR, the coolant in the fuel bundle becomes a steam-water two-phase flow, and the steam, after passing through a steam-water separator, directly drives the turbine. The plant configuration of a BWR is simpler than that of a PWR, which receives heat from the core indirectly by a secondary cooling

CONTACT Tetsuhiro Ozaki ozaki-tetsuhiro@tepsys.co.jp TEPCO Systems Corporation Shibusawa City Place Eitai, 2-37-28, Eitai, Koto, Tokyo 135-0003, Japan

© 2023 Atomic Energy Society of Japan. All rights reserved.

system. Hundreds of fuel bundles in the BWR core form independent channels by channel boxes. In these channels, the flow distribution in the core is adjusted by orifices at the inlet to appropriately cool individual fuel elements by removing generated heat. The fuel burnup proceeds by nuclear fission caused by moderated neutrons. The behaviors of neutrons, i.e. the neutron moderation characteristics, strongly depend on the coolant condition. In general, the lower the void fraction, the more effectively the neutrons are moderated and the more easily the fission occurs, resulting in higher heat power and higher burnup. Thus, the coolant conditions and the nuclear characteristics of the fuel are closely related, and understanding the thermal-hydraulic characteristics in the core is indispensable for core management, such as fuel arrangement in the core, operation planning, and stability evaluation.

In a BWR core, a channel box accommodates one fuel bundle, and thus each fuel bundle has an independent flow path. The thermal-hydraulic state of each bundle is evaluated by simulating the cross-sectional averaged axial one-dimensional flow. In general, the concentration of burnable poison (e.g. Gd_2O_3) is different for each fuel rod in the bundle because the entire core should be optimized so that the power of each bundle does not differ significantly. Therefore, the power distribution, especially at the beginning of the fuel life, is usually inhomogeneous, and the void fraction in the bundle also has a distribution. In nuclear core calculations, these inhomogeneities are usually not considered when the fuel bundles are treated one-dimensionally. If the macroscopic reaction cross-section of the bundle referred to in the nuclear physics calculation assumes that the void fraction is uniform, the difference from the actual reaction cross-section will increase because the void fraction distribution will not be uniform for fuels with a large heterogeneity of power distribution. Considering such heterogeneity in the bundle for the core design, the reliability of the simulation is expected to be increased. In recent years, fuel designs with increased heterogeneity in the bundle have been introduced for global optimization in the first-loading core [1]. In addition, during the insertion of control rods, the regional power adjacent to the control rods is greatly reduced, thus resulting in the expansion of the inhomogeneity. Therefore, it is desirable to utilize thermal-hydraulic simulations that can consider the heterogeneity directly because there are many aspects whereby the heterogeneity increases in the actual core [2].

Three-dimensional CFD is a method that can directly account for the inhomogeneity of the thermal-hydraulic state within a fuel bundle [3]. However, the use of CFD codes in boiling two-phase flows has many difficult challenges to overcome. For example, the computational time increases significantly with the increase in the number of computational cells. In the two-phase flow, the mass, momentum, and energy conservation equations must be solved for each gas–liquid phase, and the six-conservative equation system must be solved by a large number of coupled cells. For the two-phase CFD, the constitutive equations describing the behavior of the interfacial transfer are not reliable enough. Most of the constitutive equations are based on simple geometries and databases obtained under atmospheric pressure, which are not sufficiently applicable to actual conditions [4]. Although the resolution of the subchannel analysis code is coarser than that of the CFD code, the subchannel analysis code is a good option for clarifying the inhomogeneity in the bundle.

The subchannel analysis code divides the region in the fuel bundle into several channels called subchannels. When the subchannel analysis code is applied to the core conditions during normal operation or an anticipated operational occurrence (AOO), the flow in the core is assumed to be vertically upward. Therefore, the flow in the subchannels is also assumed to be dominated by the upward flow. However, it is common to consider the lateral flow, namely the cross-flow between adjacent subchannels, due to pressure difference, turbulent mixing, and void drift. With the subchannel code, parameters such as void fraction and flow velocity in the fuel bundle can be evaluated at the subchannel scale. Therefore, the inhomogeneity in the rod bundle can be evaluated in detail compared with the one-dimensional cross-sectional average code, and the effect of the inhomogeneity can be directly taken into account in the nuclear thermal coupling calculation and the thermal limit calculation.

Subchannel analysis codes have been developed and utilized as a method to simulate the core thermal-hydraulic behavior in LWRs in detail. In some cases, individual fuel bundle regions are treated as a single subchannel when simulating the entire core in a PWR. The COBRA-IV code [5] is a subchannel analysis code using the homogeneous flow model, and it has been applied to PWR simulations. A method for handling a single fuel bundle by dividing it into multiple subchannels was developed. The critical heat flux under high-quality conditions in BWRs is said to occur when the fuel rods are no longer cooled by the liquid film. This critical condition is important in determining fuel performance. One of the roles of the subchannel analysis code has been to reasonably predict the occurrence of the critical heat flux in the bundle. In the US, the COBRA-TF code [6] was developed as a successor to the COBRA-IV code, and recently, the CTF code, which is an improved version of the COBRA-TF code,

has been developed [7]. In Japan, the development of codes such as FIDAS [8], SILFEED [9], and NASCA [10] has progressed since the 1990s.

Subchannel codes for simulating thermal-hydraulic behavior in fuel bundles are useful not only for predicting the critical heat flux but also for evaluating the inhomogeneity of void fraction distribution in fuel bundles at steady power. However, most of the subchannel codes do not consider the inhomogeneity of the void fraction distribution and the velocity distribution inside the subchannels when dealing with the subchannel-averaged physical quantities.

In the one-dimensional analysis codes, including the subchannel analysis codes, cross-sectional average quantities are treated in the conservation equations. The void fraction distribution and velocity distribution in the channel can be represented by distribution parameters. By using these distribution parameters, the effect of inhomogeneity can be properly treated in simulations [11]. Therefore, it is necessary to model the distribution parameters considering the void fraction distribution and the flow velocity distribution in the subchannel scale for the subchannel analysis code. Julia et al. [12] derived the distribution parameter for subchannels using assumed void fraction and mixture volumetric flux distributions, but only for the interior subchannels. Further, the data used to validate their model was an atmospheric pressure 3×3 bundle with $D_0/P_0 = 0.5$, where D_0/P_0 is the ratio of rod outer diameter to rod pitch. The model has not been validated under actual nuclear reactor operating conditions. In addition, the subchannel geometry can be expressed by D_0/P_0 as a parameter, but the model of Julia et al. does not consider extrapolation to a large region of D_0/P_0, which is important for future fuel designs. Therefore, to carry out the subchannel analysis in the fuel bundle considering the void fraction distribution and the velocity distribution, it is necessary to (1) develop the constitutive equations for the inner, edge, and corner subchannels; (2) evaluate them under the actual thermal-hydraulic conditions; and (3) confirm the extrapolation performance. The developed model is implemented into a subchannel analysis code and analyzed to examine the effect of the improvement in prediction performance.

The NUPEC rod bundle void fraction data, described in Section 2, can be used as a reliable database to provide the void fraction distribution in the subchannels for validation [13–15]. In Section 3, a method for deriving the distribution parameter model and the constitutive equations for dispersed two-phase flows are presented. Sections 4 and 5 describe the evaluation of the developed distribution parameter model. These sections show, respectively, the applicability of the proposed model of distribution parameters that can be calculated based on the results of the NUPEC rod bundle void fraction test and the predictive ability of the calculated cross-sectional average void fraction when the proposed model is incorporated into the NASCA code.

2. Experimental database

There are several examples of experiments in which void fraction in simulated fuel bundles (or fuel bundle simulators) was measured. In this paper, NUPEC rod bundle void fraction test data [13–15] were selected as a database for model evaluation for the following reasons.

- In addition to the cross-sectional average void fraction of the fuel bundle simulator, the void fraction distribution in each subchannel was measured.
- The geometry of the fuel bundle simulator was the same as the prototypic BWR fuel bundle.
- The test conditions included the high-temperature and high-pressure conditions of the actual BWR.

Figure 1 shows the test loop and the cross-sectional shape of the fuel bundle simulator used in the NUPEC rod bundle void fraction test. The test bundle simulator has the geometry of the 8×8 fuel bundle loaded in the actual BWR. The outer diameter and rod pitch of the heating rod are 12.3 mm and 16.2 mm, respectively. The channel box of the fuel bundle simulator is a square of 132.5 mm in inner dimension with a curvature at the corner. The fuel bundle simulator is stored in this square channel box. The rods are electrically heated to simulate the fission heat generation in the actual reactor. The heated length of the simulator is 3.7 m, which is the same as that of the actual fuel. The fuel bundle simulator is connected to a closed loop that separates and condenses the steam generated by the simulator heating and returns it to the fuel bundle simulator at a predetermined flow rate. This test loop has a pressurizer that can control the steam flow rate to simulate the prototypic BWR operating pressure condition.

The coolant flowing into the fuel bundle simulator from the entrance of the simulator becomes a boiling two-phase flow due to the heat transfer from the heating rod in the bundle. When the two-phase flow reaches the upper end of the heating section, the void fraction is measured by X-ray CT. The X-ray CT system consists of an X-ray tube and 512 detectors that emit a fan-shaped beam and receive the beam after it passes through the simulator. The X-ray tube and detectors rotate around the fuel bundle simulator synchronously with each other, and the detection

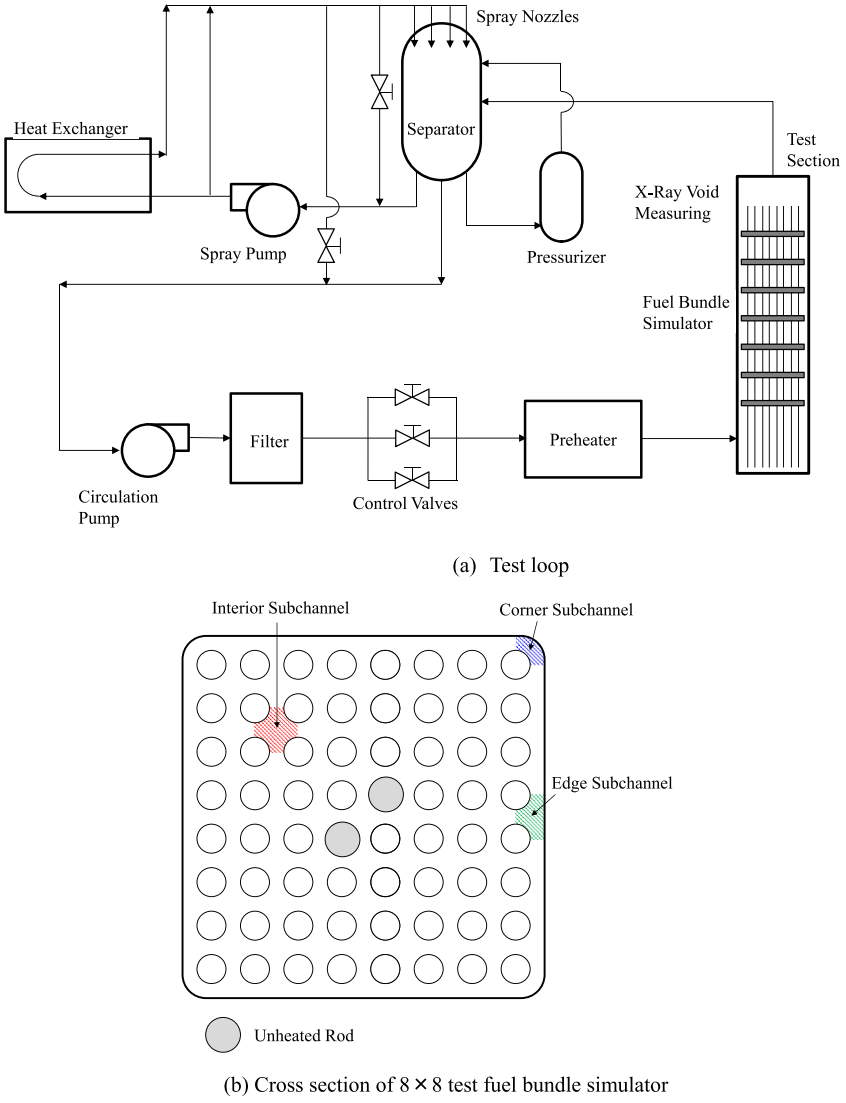

Figure 1. Test loop and cross section of 8 × 8 test fuel bundle simulator used in the NUPEC test.

signal is converted into the void fraction at the local position using the process computer.

The local void fraction measured by the X-ray CT is numerically processed into the cross-sectional average void fraction of the whole fuel bundle simulator and the average void fraction of each subchannel. Figure 1(b) shows a typical interior subchannel, edge subchannel, and corner subchannel. The interior subchannel, which is surrounded by four rods, is a subchannel in the center of the fuel bundle simulator. The edge subchannel is a subchannel in the region bounded by two rods and the casing wall of the fuel bundle simulator. The corner subchannel is a subchannel in the region bounded by one rod and the casing wall in each of the four corners of the fuel bundle simulator. The accuracy of the measurement of the void fraction in the fuel bundle simulator is 3% on average for the subchannel void fraction [16].

Among the NUPEC rod bundle void fraction test data, the test case (Run-1) is used as the database for the model evaluation shown in Sections 4 and 5. In the test case, unheated rods simulate the water rod of the actual fuel bundle. The outer diameter of the unheated rods is 15 mm. The axial and radial power distribution is uniform. The pressure conditions are 1.0, 3.9, 7.2, and 8.6 MPa, and the mass flux ranges from 280 to 2000 kg/m^{2}s. The total bundle power is set by adjusting the quality at the upper end of the heating section to be in the range between 0 and 0.25. In the test case Run-1, a total of 86 test conditions are measured. The number of interior subchannels, edge subchannels, and corner subchannels is 49, 28, and 4, respectively, in an 8 × 8 fuel bundle. Therefore, the number of data points for each subchannel is 4214, 2408, and 344 for the interior subchannel, edge subchannel, and corner subchannel, respectively.

3. Modeling

3.1. Formulation of interfacial drag force in subchannels

In the simulation of a gas–liquid two-phase flow in a subchannel, the conservation equations are averaged

over the subchannel cross-section. In the momentum conservation equation averaged over the subchannel cross-section, which is important for predicting the void fraction, the momentum exchange between the gas and liquid phase interfaces is caused by the interfacial drag force. The cross-sectional average interfacial drag force at the subchannel is expressed as [11],

$$\langle M_{ig}\rangle_p = -\langle M_{if}\rangle_p = -\frac{1}{8}\langle a_i\rangle_p C_D \rho_f \psi \langle v_r\rangle_p \left|\langle v_r\rangle_p\right|, \tag{1}$$

where M_{ik},a_i,C_D,ρ_f, ψ, and v_r are the interfacial drag force acting on the k-phase (k=g, gas; k=f, liquid), interfacial area concentration, drag coefficient, liquid density, shape factor, and the relative velocity between gas and liquid phases, respectively. $<>_p$ denotes the cross-sectional average quantity of a subchannel type p, i.e. p = c, e, or i, representing the corner, edge, and interior subchannels, respectively. The cross-sectional average relative velocity appearing in Equation (1) is expressed as [17],

$$\langle v_r\rangle_p \simeq \frac{1 - C_{0,p}\langle\alpha\rangle_p}{1 - \langle\alpha\rangle_p}\langle\langle v_g\rangle\rangle_p - C_{0,p}\langle\langle v_f\rangle\rangle_p, \tag{2}$$

where C_0, α, v_g, and v_f represent the distribution parameter, void fraction, gas phase velocity, and liquid phase velocity, respectively. $<<>>_p$ represents the void fraction weighted mean volume of subchannel type p. Since the distribution parameter depends on the geometry, it is expressed as follows for the corner, edge, and interior subchannel types [11],

$$C_{0,p} \equiv \frac{\langle\alpha j\rangle_p}{\langle\alpha\rangle_p\langle j\rangle_p}, \tag{3}$$

where j is the mixture volumetric flux.

From the definition of Equation (3), if the void fraction distribution and mixture volumetric flux distribution are known, the distribution parameter can be calculated. As for the mixture volumetric flux distribution, it is known that the power-law distribution with the seventh power law is a good approximation for an interior subchannel [12]. This approximation is also applied to edge and corner subchannels. Since the contribution of void fraction distribution (i.e. wall peaking or core peaking) to the distribution parameter is generally more important, this approximation for the mixture volumetric flux may not significantly affect the calculated distribution parameter. The void fraction distribution shows a characteristic change depending on the flow condition. In bulk boiling, the power-law distribution gives a good approximation, but in subcooled boiling, the void fraction peak occurs near the heating wall. The void fraction in the subcooled boiling condition can be assumed uniform in the bubble layer near the heating wall [18]. The bubble layer thickness model can be applied to derive the distribution parameter numerically.

In the critical pressure condition, the void fraction distribution is assumed to be uniform because the inertia of both phases is equivalent. Therefore, the void fraction distribution in bulk boiling is pressure dependent, and the exponent of the power-law distribution becomes larger as the pressure increases. In this paper, instead of expressing the exponent of the power-law distribution of the void fraction in terms of pressure or density ratio, the distribution parameter, $C_{0,\infty,p}$, without considering the pressure effect is calculated. Then, the effect of pressure on $C_{0,p}$ is modeled by the following equation [19],

$$C_{0,p} = C_{0,\infty,p} - \left(C_{0,\infty,p} - 1\right)\sqrt{\frac{\rho_g}{\rho_f}}, \tag{4}$$

where ρ_g is the gas phase density.

3.2. Modeled distributions of void fraction and mixture volumetric flux in subchannels

To calculate the distribution parameter from Equation (3), the void fraction distribution and mixture volumetric flux distribution are required. Flow channel geometries such as subchannel type affect the void fraction distribution and mixture volumetric flux distribution. Thermal conditions, such as subcooled boiling and bulk boiling conditions, also affect the distributions. The void fraction distribution and mixture volumetric flux distribution are formulated by considering these factors affecting the distributions as follows.

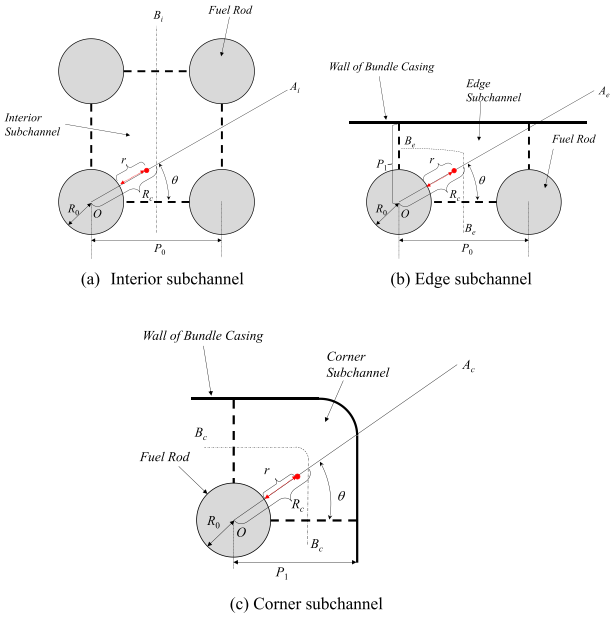

Figure 2. Modeled coordinate of (a) interior subchannel, (b) edge subchannel, and (c) corner subchannel.

3.2.1. Interior subchannel

3.2.1.1. Bulk boiling region. In this study, the mixture volumetric flux distribution for dispersed two-phase flows in the interior subchannel shown in Figure 2(a) is assumed as follows [12, 20]:

$$j(r,\theta) = j_{c,i}(\theta)\left\{1 - \left|1 - \frac{2r}{R - R_0}\right|^{m_j}\right\} \text{ for } 0 \le r \le R_c - R_0; 0 \le \theta \le \frac{\pi}{4}, \quad (5)$$

where r and θ are the coordinates of the radial and circumferential directions, respectively. The r represents the distance from the rod surface whose radius is R_0 and m_j is the exponent for the mixture volumetric flux. The position of $r = (R\text{-}R_0)/2$ represents the 'hypothetical' center of the channel between $r = R - R_0$ and $r = 0$. $j_{c,i}(\theta)$ represents the maximum mixture volumetric flux on line A_i in Figure 2(a) and R is defined as follows.

$$R \equiv 2R_c - R_0 \quad (6)$$

R_c is the distance from the origin to the point where the mixture volumetric flux is the maximum. Line B_i in Figure 2(a) is the midline between the adjacent rods, so the maximum value of the mixture volumetric flux along line A_i appears on line B_i. R_c is the distance from the rod center to the intersection of line A_i and line B_i, and it is expressed by the following equation,

$$R_c = \frac{(P_0/2)}{\cos\theta}, \quad (7)$$

where P_0 is the rod pitch. Substituting R determined from Equation (6) and Equation (7) into Equation (5), the mixture volumetric flux is expressed as Equation (8).

$$j(r,\theta) = j_{c,i}(\theta)\left\{1 - \left|1 - \frac{2r\cos\theta}{P_0 - 2R_0\cos\theta}\right|^{m_j}\right\}. \quad (8)$$

Next, $j_{c,i}(\theta)$ is modeled. The mixture volumetric flux along the line $\theta = \theta' = \pi/4$ can be written as Equation (9). Here, θ' is the angle where the maximum value of the mixture volumetric flux occurs. The mixture volumetric flux is assumed to take maximum in the interior subchannel along the line $\theta = \theta' = \pi/4$.

$$j\left(r,\frac{\pi}{4}\right) = j_{c0,i}\left\{1 - \left|1 - \frac{2r}{\sqrt{2}P_0 - 2R_0}\right|^{m_j}\right\}. \quad (9)$$

Here, $j_{c0,i}$ is the mixture volumetric flux at the center point of the interior subchannel. The r on line B_i is expressed by the following equation.

$$r = \frac{(P_0/2)}{\cos\theta} - R_0. \quad (10)$$

Therefore, the mixture volumetric flux on line B_i can be expressed by substituting Equation (10) into Equation (9) as follows.

$$j_{c,i}(\theta) = j_{c0,i}\left\{1 - \left|1 - \frac{P_0 - 2R_0\cos\theta}{\left(\sqrt{2}P_0 - 2R_0\right)\cos\theta}\right|^{m_j}\right\}. \quad (11)$$

Substituting Equation (11) into Equation (8), the mixture volumetric flux can be expressed as follows.

$$j(r,\theta) = j_{c0,i}\left\{1 - \left|1 - \frac{P_0 - 2R_0\cos\theta}{\left(\sqrt{2}P_0 - 2R_0\right)\cos\theta}\right|^{m_j}\right\}\left\{1 - \left|1 - \frac{2r\cos\theta}{P_0 - 2R_0\cos\theta}\right|^{m_j}\right\} \quad (12)$$
$$\text{for } 0 \le r \le R_c - R_0; 0 \le \theta \le \frac{\pi}{4}.$$

The void fraction distribution for dispersed two-phase flows is derived in the same way as in Equation (12) and is expressed by,

$$\alpha(r,\theta) = \alpha_{c0,i}\left\{1 - \left|1 - \frac{P_0 - 2R_0\cos\theta}{\left(\sqrt{2}P_0 - 2R_0\right)\cos\theta}\right|^{m_\alpha}\right\}\left\{1 - \left|1 - \frac{2r\cos\theta}{P_0 - 2R_0\cos\theta}\right|^{m_\alpha}\right\}$$
$$\text{for } 0 \le r \le R_c - R_0; 0 \le \theta \le \frac{\pi}{4}, \quad (13)$$

where m_α is the exponent for the void fraction distribution, $\alpha_{c0,i}$ is the void fraction on line B_i at $\theta = \theta' = \pi/4$, and it is the maximum value in the interior subchannel.

3.2.1.2. Subcooled boiling region. The mixture volumetric flux distribution in the subcooled boiling region is assumed to be similar to that in bulk boiling [18]. In the subcooled boiling, bubbles are concentrated around the heating rod, and the center region of the subchannel becomes a liquid single-phase. Therefore, the void fraction becomes larger near the heating wall as shown in Figure 3(a). The void fraction distribution in this subcooled boiling is approximated as shown in Figure 3(b). It is divided into a region where bubbles are concentrated within the distance x_{wp} from the rod surface and a region with zero void fraction outside x_{wp}. Applying the idea of the bubble layer thickness model [18] allows the void fraction distribution during subcooled boiling to be expressed by the following.

$$\begin{aligned} \alpha &= \alpha_{wp} \quad \text{for} \quad 0 \le r \le x_{wp} \\ \alpha &= 0 \quad \text{for} \quad x_{wp} < r \le R_c - R_0 \end{aligned}. \quad (14)$$

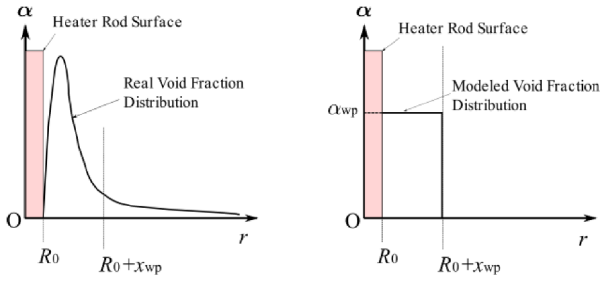

(a) Subcooled boiling flow (b) Modeled subcooled boiling low

Figure 3. Real and modeled void fraction distribution for subcooled boiling flow.

3.2.2. Edge subchannel

3.2.2.1. Bulk boiling region. The mixture volumetric flux distribution for dispersed two-phase flows in the edge subchannel shown in Figure 2(b) is approximated as shown in the following equation.

$$j(r,\theta) = j_{c,e}(\theta)\left\{1 - \left|1 - \frac{2r}{R - R_0}\right|^{m_j}\right\},$$
$$0 \le r \le R_c' - R_0;\ 0 \le \theta \le \frac{\pi}{2} \tag{15}$$

$$\begin{cases} R_c' = \frac{P_0}{2\cos\theta} \text{ for } \theta \le \tan^{-1}\left(\frac{P_1}{P_0/2}\right) \\ R_c' = \frac{P_1}{\sin\theta} \text{ for } \theta > \tan^{-1}\left(\frac{P_1}{P_0/2}\right) \end{cases}. \tag{16}$$

Here, P_1 is the distance from the rod center point to the channel wall. As in the case of the interior subchannel, j computed in Equation (15) becomes $j = 0$ at the position of $r = 0$ or $R - R_0$, and maximum at $r = (R\text{-}R_0)/2$. $j_{c,e}(\theta)$ denotes the maximum mixture volumetric flux on line A_e in Figure 2(b). The definition of R is the same as in Equation (6). R_c in Equation (6) is the distance from the center of the rod to the point where the mixture volumetric flux is the maximum. For the edge subchannel, the distance R_c depends on whether the closest wall is a neighboring rod or the wall of the bundle casing. The distance R_c is calculated as follows.

$$R_c = \frac{(P_0/2)}{\cos\theta} \text{ for } \theta \le \theta_0,$$
$$R_c = \left(\frac{P_1}{\sin\theta} - R_0\right)/2 + R_0 = \frac{P_1}{2\sin\theta} + \frac{R_0}{2} \text{ for } \theta > \theta_0. \tag{17}$$

Here, θ_0 is the angle at which the two R_c terms in Equation (17) are equal. Substituting Equation (17) into Equation (6) and substituting the resulting R into Equation (15) lead to the following expressions.

$$j(r,\theta) = j_{c,e}(\theta)\left\{1 - \left|1 - \frac{2r\cos\theta}{P_0 - 2R_0\cos\theta}\right|^{m_j}\right\} \text{ for } \theta \le \theta_0,$$
$$j(r,\theta) = j_{c,e}(\theta)\left\{1 - \left|1 - \frac{2r\sin\theta}{P_1 - R_0\sin\theta}\right|^{m_j}\right\} \text{ for } \theta > \theta_0. \tag{18}$$

Next, $j_{c,e}(\theta)$ is modeled. The location where the maximum value of mixture volumetric flux occurs depends on the angle θ. Here, the angle where the maximum value of the mixture volumetric flux occurs is denoted by θ'. For $\theta' \le \theta_0$, the maximum value of the mixture volumetric flux occurs at the intersection of line A_e and the equidistant line from the adjacent rods. For $\theta' \ge \theta_0$, the maximum value of mixture volumetric flux occurs at the midpoint between the rod surface and the channel wall on line A_e. Line B_e in Figure 2(b) shows the point where the maximum value of mixture volumetric flux occurs. The distribution of the mixture volumetric flux on line A_e with angle θ' is expressed by the following equation.

$$j(r,\theta') = j_{c0,e}\left\{1 - \left|1 - \frac{2r\cos\theta'}{P_0 - 2R_0\cos\theta'}\right|^{m_j}\right\} \text{ for } \theta' \le \theta_0,$$
$$j(r,\theta') = j_{c0,e}\left\{1 - \left|1 - \frac{2r\sin\theta'}{P_1 - R_0\sin\theta'}\right|^{m_j}\right\} \text{ for } \theta' > \theta_0. \tag{19}$$

The r coordinate of line B_e is the distance from the center of the rod to the point where the mixture volumetric flux is the maximum, which is R_c in Equation (17) itself. Therefore, R_c-R_0 is substituted into r in Equation (19), and the mixture volumetric flux on line B_e is expressed as follows,

$$j_{c,e}(\theta) = j_{c0,e}\left\{1 - \left|1 - \frac{2\{(P_0/2) - R_0\cos\theta\}\cos\theta_0}{(P_0 - 2R_0\cos\theta_0)\cos\theta}\right|^{m_j}\right\} \text{ for } \theta \le \theta_0,$$
$$j_{c,e}(\theta) = j_{c0,e}\left\{1 - \left|1 - \frac{(P_1 - R_0\sin\theta)\cos\theta_0}{(P_0 - 2R_0\cos\theta_0)\sin\theta}\right|^{m_j}\right\} \text{ for } \theta > \theta_0. \tag{20}$$

where $j_{c0,e}$ is the mixture volumetric flux on line B_e at $\theta = \theta' = \theta_0$%*MathType!End!2!1!for*$\theta > \theta_0$. and the maximum value of j in the edge subchannel. From Equations (18) and (20), the volumetric flux distribution is expressed as Equation (21).

$$j(r,\theta) = j_{c0,e}\left\{1 - \left|1 - \frac{2\{(P_0/2) - R_0\cos\theta\}\cos\theta_0}{(P_0 - 2R_0\cos\theta_0)\cos\theta}\right|^{m_j}\right\}$$
$$\left\{1 - \left|1 - \frac{2r\cos\theta}{P_0 - 2R_0\cos\theta}\right|^{m_j}\right\} \text{for } \theta \le \theta_0$$
$$j(r,\theta) = j_{c0,e}\left\{1 - \left|1 - \frac{(P_1 - R_0\sin\theta)\cos\theta_0}{(P_0 - 2R_0\cos\theta_0)\sin\theta}\right|^{m_j}\right\}$$
$$\left\{1 - \left|1 - \frac{2r\sin\theta}{P_1 - R_0\sin\theta}\right|^{m_j}\right\} \text{ for } \theta > \theta_0. \tag{21}$$

The void fraction distribution for dispersed two-phase flows is assumed to be derived in the same way as in Equation (21) and is expressed by,

$$\alpha(r,\theta) = \alpha_{c0,e}\left\{1 - \left|1 - \frac{2\{(P_0/2) - R_0\cos\theta\}\cos\theta_0}{(P_0 - 2R_0\cos\theta_0)\cos\theta}\right|^{m_\alpha}\right\}$$
$$\left\{1 - \left|1 - \frac{2r\cos\theta}{P_0 - 2R_0\cos\theta}\right|^{m_\alpha}\right\} \text{for } \theta \le \theta_0$$
$$\alpha(r,\theta) = \alpha_{c0,e}\left\{1 - \left|1 - \frac{(P_1 - R_0\sin\theta)\cos\theta_0}{(P_0 - 2R_0\cos\theta_0)\sin\theta}\right|^{m_\alpha}\right\}$$
$$\left\{1 - \left|1 - \frac{2r\sin\theta}{P_1 - R_0\sin\theta}\right|^{m_\alpha}\right\} \text{for } \theta > \theta_0, \tag{22}$$

where $\alpha_{c0,e}$ is the void fraction on line B_e at θ=θ' and it is the maximum value in the edge subchannel.

3.2.2.2. Subcooled boiling region. The mixture volumetric flux distribution in the subcooled boiling region is assumed by Equation (21). The void fraction distribution is assumed by Equation (23) using the bubble layer thickness model as well as the interior subchannel.

$$\begin{aligned} \alpha &= \alpha_{wp} \quad \text{for} \quad 0 \le r \le x_{wp} \\ \alpha &= 0 \quad\ \ \text{for} \quad x_{wp} < r \le R_c' - R_0. \end{aligned} \tag{23}$$

3.2.3. Corner subchannel

3.2.3.1. Bulk boiling region. The mixture volumetric flux distribution for dispersed two-phase flows in the corner subchannel shown in Figure 2(c) is approximated as shown in the following equation.

$$j(r,\theta) = j_{c,c}(\theta)\left\{1 - \left|1 - \frac{2r}{R - R_0}\right|^{m_j}\right\} \quad \text{for } 0 \le r \le R - R_0\,; 0 \le \theta \le \frac{\pi}{2}. \tag{24}$$

As in the case of the interior subchannel, j computed in Equation (24) becomes $j = 0$ at the position of $r = 0$ or $R - R_0$, and maximum at $r = (R\text{-}R_0)/2$. $j_{c,c}(\theta)$ denotes the maximum mixture volumetric flux on line A_c in Figure 2(c). The definition of R is the same as in Equation (6), where R_c in Equation (6) is the distance from the center of the rod to the point where the mixture volumetric flux is maximum. The maximum mixture volumetric flux on line A_c is assumed to be the midpoint between the rod surface and the channel wall. Therefore, R can be expressed by the following equation.

$$R = \frac{P_1}{\cos\theta} \tag{25}$$

Substituting Equation (25) into Equation (24), the mixture volumetric flux can be expressed as the following.

$$j(r,\theta) = j_{c,c}(\theta)\left\{1 - \left|1 - \frac{2r\cos\theta}{P_1 - R_0\cos\theta}\right|^{m_j}\right\}. \tag{26}$$

Next, $j_{c,c}(\theta)$ is modeled. $j_{c,c}(\theta)$ is the maximum mixture volumetric flux on line A_c in Figure 2(c). This is the mixture volumetric flux on the midpoint of the distance from the rod surface to the channel wall. On the line θ=θ'=π/4, the mixture volumetric flux is expressed as,

$$j\left(r,\frac{\pi}{4}\right) = j_{c0,c}\left\{1 - \left|1 - \frac{2r}{\sqrt{2}P_1 - R_0}\right|^{m_j}\right\}, \tag{27}$$

where $j_{c0,c}$ is the maximum value of the mixture volumetric flux on the line θ=θ'=π/4. The position r where the mixture volumetric flux has its maximum value on line A_c is R_c itself and is expressed by the following equation.

$$r = \frac{P_1}{2\cos\theta} - \frac{R_0}{2}. \tag{28}$$

Therefore, $j_{c,c}(\theta)$ is expressed by substituting r obtained by Equation (28) into Equation (26).

$$j_{c,c}(\theta) = j_{c0,c}\left\{1 - \left|1 - \frac{P_1 - R_0\cos\theta}{\left(\sqrt{2}P_1 - R_0\right)\cos\theta}\right|^{m_j}\right\} \tag{29}$$

From Equations (26) and (29), the mixture volumetric flux distribution can be expressed as the following.

$$j(r,\theta) = j_{c0,c}\left\{1 - \left|1 - \frac{P_1 - R_0\cos\theta}{\left(\sqrt{2}P_1 - R_0\right)\cos\theta}\right|^{m_j}\right\} \left\{1 - \left|1 - \frac{2r\cos\theta}{P_1 - R_0\cos\theta}\right|^{m_j}\right\} \quad \text{for } 0 \le r \le R - R_0\,;\, 0 \le \theta \le \frac{\pi}{2}. \tag{30}$$

The void fraction distribution for dispersed two-phase flows is derived in the same way as in Equation (30) and is expressed by,

$$\alpha(r,\theta) = \alpha_{c0,c}\left\{1 - \left|1 - \frac{P_1 - R_0\cos\theta}{\left(\sqrt{2}P_1 - R_0\right)\cos\theta}\right|^{m_\alpha}\right\} \left\{1 - \left|1 - \frac{2r\cos\theta}{P_1 - R_0\cos\theta}\right|^{m_\alpha}\right\} \quad \text{for } 0 \le r \le R - R_0\,; 0 \le \theta \le \frac{\pi}{2}, \tag{31}$$

where $\alpha_{c0,c}$ is the void fraction at $\theta = \theta' = \pi/4$ and is the maximum value of the void fraction in the corner subchannel.

3.2.3.2. Subcooled boiling region. The mixture volumetric flux distribution in the subcooled boiling region is assumed by Equation (30). The void fraction distribution is assumed by Equation (32) using the bubble layer thickness model.

$$\alpha = \alpha_{wp} \text{ for } 0 \le r \le x_{wp}, \quad \alpha = 0 \text{ for } x_{wp} < r \le R - R_0. \tag{32}$$

3.3. Modeling of the distribution parameter for bulk boiling flow

3.3.1. Modeling strategy

Based on the void fraction and mixture volumetric flux distributions assumed in Section 3.2, once m_j, m_α, and bundle geometries are determined, the distribution parameter can be calculated using the definition in Equation (3). The assumed void fraction and mixture volumetric flux distributions are applicable to rods arranged in a square lattice. The geometry of each subchannel is determined by the rod outer diameter D_0, the rod pitch P_0, and the distance P_1 between the wall of the outermost rod adjacent to the channel wall. The geometrical dimensions of representative BWR fuel bundles are given in Table 1 [21–23]. The following steps are used to calculate the distribution parameter by characterizing the bundle geometry with a parameter such as D_0/P_0.

(1) The terms m_j and m_α are assumed, and their values are justified by sensitivity analysis.

Table 1. Geometrical dimensions of representative BWR fuel bundles [21–23].

	8 × 8 (NUPEC)	9 × 9 (Type-A)	9 × 9 (Type-B)	10 × 10 (GE14)
Rod diameter [cm], D_0	1.23	1.12	1.10	1.026
Rod pitch [cm], P_0	1.62	1.43	1.43	1.295
Wall to rod distance [cm], P_1	.975	.905	.905	0.873
D_0/P_0 [-]	.759	.783	.769	0.792
R_0/P_1 [-]	.631	.619	.608	0.588
k	.923	1.11	1.08	1.34

(2) The void fraction and mixture volumetric flux distributions in the bulk boiling region described in Section 3.2 are applied for different D_0/P_0 and P_1 conditions. Then, C_∞ is calculated numerically.
(3) C_∞ is given as a function of geometric parameters such as D_0/P_0.

The following assumption is applied for step (1) of the above procedure. The value of m_j was estimated by Yun et al. [24]. Based on their experimental data, Julia [12] showed that $m_j = 7$ was a good approximation under atmospheric conditions. In addition, it can be confirmed that the sensitivity of m_α to the calculation of the distribution parameter using Equations (3), (12), and (13) is not significant in the vicinity of $m_\alpha = 7$, as shown in Figure 4. Therefore, $m_j = m_\alpha = 7$ can be assumed in the subsequent derivation. The distribution parameter determined under the assumption of $m_j = 7$ and $m_\alpha = 7$ is considered to be the asymptotic distribution parameter C_∞. As discussed in section 3.1, the exponent m_α should increase as the pressure or density ratio increases. The pressure effect on the distribution parameter is modeled by Equation (4). Steps (2) and (3) are described next.

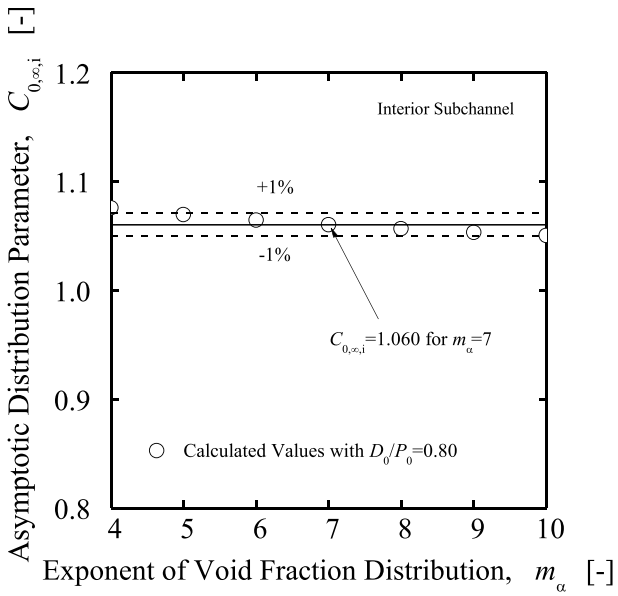

Figure 4. Dependency of distribution parameter to exponent of void fraction distribution, m_α.

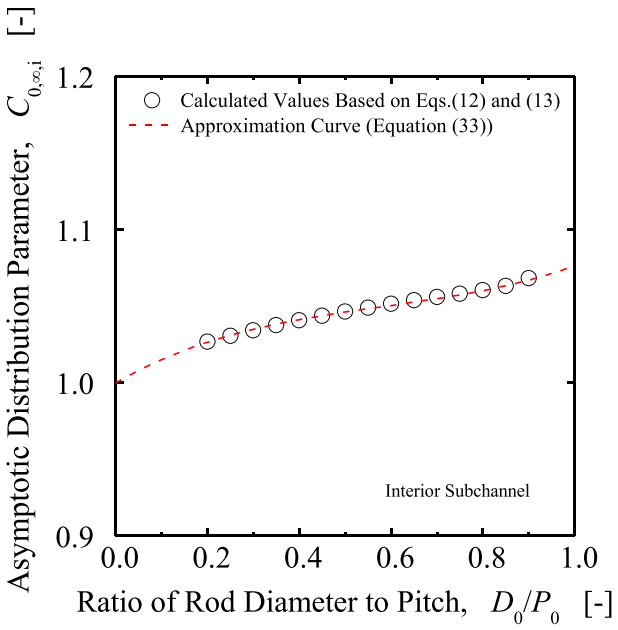

Figure 5. Calculated and approximated distribution parameter for interior subchannel.

3.3.2. Distribution parameter for bulk boiling flow

3.3.2.1. Interior subchannel. The distribution parameter defined in Equation (3) is calculated numerically in the range of $0.2 \le D_0/P_0 \le 0.9$ to include the design range of BWR fuel bundles shown in Table 1. Figure 5 shows the variation of the distribution parameter relative to D_0/P_0. For convenience, the calculated distribution parameters are correlated by a function of D_0/P_0 as,

$$C_{0,\infty,i} = 0.9999 + 0.1717(D_0/P_0) - 0.2215(D_0/P_0)^2 + 0.1263(D_0/P_0)^3. \quad (33)$$

3.3.2.2. Edge subchannel. The geometry of the edge subchannel depends not only on D_0/P_0 but also on the distance P_1 between the rod and the channel wall. To consider the effect of P_1 on the distribution parameter, the ratio of the distance between the rod and the channel wall to the gap width between rods, k, is defined. The sensitivity of k to the distribution parameter is checked.

$$k \equiv \frac{P_1 - R_0}{P_0 - D_0}. \quad (34)$$

In BWR fuel bundles, the design should not be such that P_1 is much smaller than the inter-rod gap width to avoid the reduction of thermal margin for the outermost fuel rods. On the other hand, if P_1 is too large, the bias of the bundle arrangement in the channel box may become significant. In general, k is designed as a value close to 1. Therefore, the sensitivity evaluation for the distribution parameter should be performed in the range of $0.9 \le k \le 2.0$.

As shown in Figure 6, the sensitivity of the distribution parameter to k is sufficiently small. Therefore, the distribution parameter of the edge subchannel can be approximated as a function of D_0/P_0 only by the following equation.

$$C_{0,\infty,e} = 1.036 + 0.07044(D_0/P_0) - 0.08637(D_0/P_0)^2 + 0.05053(D_0/P_0)^3. \quad (35)$$

3.3.2.3. Corner subchannel. The mixture volumetric flux and void fraction distributions are given according to Equations (30) and (31), respectively. In the design of BWR fuel bundles, it is common to add curvature to the corner of the channel box. Since the radius of this corner curvature is generally about 10 mm, the difference with P_1 shown in Table 1 is small. Therefore, the distribution parameter of the corner subchannel is derived, assuming that this curvature is equal to P_1. The geometry of the corner subchannel is determined by the ratio of the rod radius R_0 to P_1. The upper limit of R_0/P_1 is set as 0.8, which is enough to cover the representative BWR fuel bundle designs.

Figure 7 shows the variation of the distribution parameter relative to R_0/P_1. The distribution parameter of the corner subchannel shown in Figure 7 can be approximated as a function of R_0/P_1 by Equation (36).

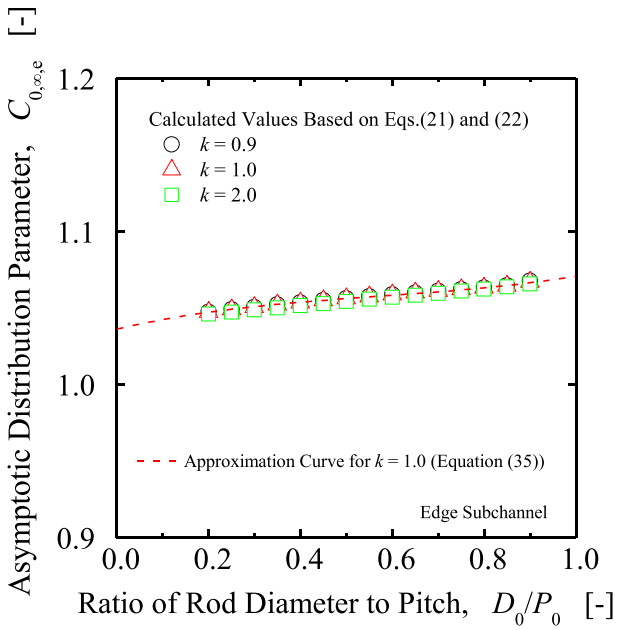

Figure 6. Calculated and approximated distribution parameter for edge subchannel.

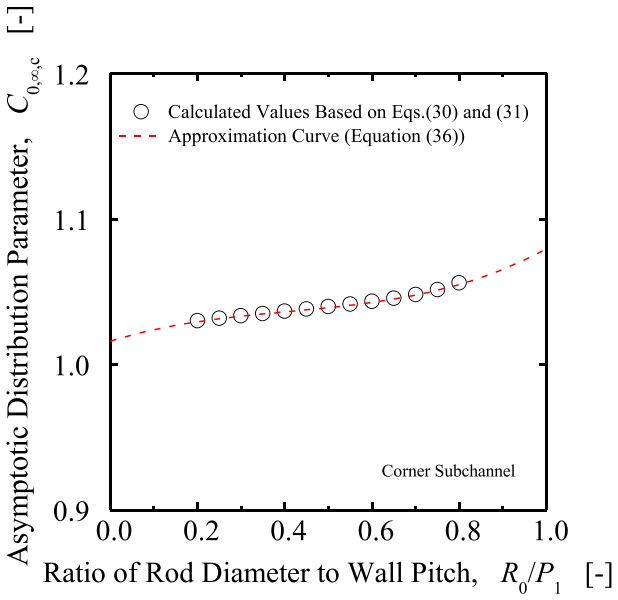

Figure 7. Calculated and approximated distribution parameter for corner subchannel.

$$C_{0,\infty,c} = 1.016 + 0.09392(R_0/P_1) - 0.1606(R_0/P_1)^2 + 0.1304(R_0/P_1)^3. \quad (36)$$

3.4. Modeling of distribution parameter for subcooled boiling flow

The distribution parameter of the subcooled boiling region is modeled according to the following steps.

(1) The assumed void fraction and mixture volumetric flux distributions in the subcooled boiling region are applied to numerically calculate $C_{0,\infty,p}$ in the same region using the bubble layer thickness model outlined in Section 3.4.1. The calculation is carried out by varying the bubble layer thickness. In addition, the relationship between the bubble layer thickness and the cross-sectional average void fraction of the subchannel is related using the concept of the bubble layer thickness model, and the relationship between the void fraction and the distribution parameter is derived.

(2) The distribution parameter in the subcooled boiling region asymptotically approaches zero as the subchannel average void fraction asymptotically approaches zero, and as the void fraction increases, the flow pattern approaches that of bulk boiling. The distribution parameter of

the subcooled boiling region obtained in step (1) is approximated by the following equation.

$$C_{0,\infty} = C_{0,\infty,\text{Bulk Boling}}\left(1 - e^{-a\langle\alpha\rangle^b}\right). \quad (37)$$

Here, a and b are determined from the distribution parameter obtained in step (1).

3.4.1. Bubble layer thickness model

The calculation method of the distribution parameters using the bubble layer thickness model [18] is outlined in Figure 8. The distribution parameter of the subcooled boiling region can be calculated by giving the void fraction distributions of the inner subchannel, edge subchannel, and corner subchannel of Equations (14), (23), and (32), respectively. The mixture volumetric flux distributions are given by Equations (12), (21), and (30), respectively. To obtain the distribution parameter in Equation (37), it is necessary to relate the thickness of the bubble layer thickness to the cross-sectional average void fraction. Hibiki et al. [18] derived the distribution parameter of the subcooled boiling region for an annulus tube using the bubble layer thickness model. The bubble layer thickness model is applied to derive the distribution parameter for the subchannel by the following procedure.

The distribution parameter, including the subcooled boiling region for a round tube, is given by the following equation based on the experimental database [19].

$$C_{0,\infty,rt} = 1.2\left(1 - e^{-18\langle\alpha\rangle}\right). \quad (38)$$

The distribution parameter of a round tube, which is determined according to the void fraction obtained by Equation (38), is used to express the distribution parameter of the subchannel by the following equation.

$$C_{0,\infty,p} = \Lambda \times C_{0,\infty,rt}. \quad (39)$$

If the void fraction distribution is given by Equations (14), (23), or (32), depending on the subchannel type, the distribution parameter for both the round tube and the subchannel channel can be obtained numerically. If the ratio of these two distribution parameters is determined as Λ, the distribution parameter of the subchannel can be calculated considering the difference in geometry by multiplying Λ by Equation (38).

To calculate Λ, the bubble layer thickness needs to be determined for both the round tube and the subchannel. The bubble layer thickness in the round tube can be calculated from the following equation by specifying the ratio of the area occupied by the bubble layer to the total channel area, A_{wp}/A_c.

$$\frac{A_{wp}}{A_c} = 1 - \left(1 - \frac{x_{wp}}{R_p}\right)^2. \quad (40)$$

Here, R_p is the radius of the round tube. Similarly, the bubble layer thickness for each subchannel type can be calculated by setting A_{wp}/A_c from the following relationship.

$$\frac{A_{wp}}{A_c} = \begin{cases} \dfrac{\pi\left(x_{wp}^2 + D_0 x_{wp}\right)}{P_0^2 - \pi\left(D_0/2\right)^2} & \text{for interior subchannel} \\ \dfrac{\pi\left(x_{wp}^2 + D_0 x_{wp}\right)}{2P_0P_1 - \pi(D_0/2)^2} & \text{for edge subchannel} \\ \dfrac{x_{wp}^2 + 2R_0 x_{wp}}{P_1^2 - R_0^2} & \text{for corner subchannel} \end{cases} \quad (41)$$

For the same A_{wp}/A_c, the distribution parameters are numerically calculated for both the round tube and the subchannel using the bubble layer thickness obtained from Equations (40) and (41), and the ratio of the two distribution parameters is set as Λ. If Λ is evaluated by varying A_{wp}/A_c, the distribution parameter of the subchannel can be calculated from Equations (38) and (39) with the void fraction as a parameter.

3.4.2. Distribution parameter for subcooled boiling flow

The bubble layer thickness is varied, and the variation of the distribution parameter to the void fraction is calculated numerically using the procedure shown in Section 3.4.1. The distribution parameter of the subchannel is approximated by Equation (37), and the coefficients a and b are obtained to reproduce the numerical results.

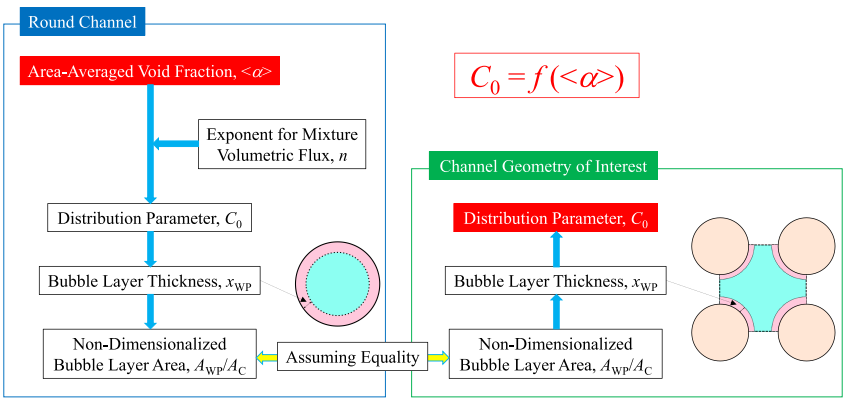

Figure 8. Overview of the method for identifying distribution parameter for a subchannel using bubble layer thickness model.

Therefore, coefficients a and b are obtained by changing D_0/P_0 or P_1 in the same way as in the case of bulk boiling in Section 3.3, and these coefficients are assumed to be functions depending only on the geometry.

3.4.2.1. Interior subchannel. The variation of the coefficients a and b in Equation (37) to D_0/P_0 can be approximated as an expression that reproduces the results of the numerical analysis as follows.

$$a = 24.87\exp\{-3.686(D_0/P_0)\} + 14.95 \\ b = 0.7731 \quad (42)$$

The distribution parameters are obtained by using Equation (33) as the distribution parameter for bulk boiling and using Equations (37) and (42) to approximate the numerical calculation with an arbitrary D_0/P_0 ranging from 0.2 to 0.9. Figure 9(a) compares analytical values to the distribution parameter calculated by Equations (33), (37), and (42) for a typical D_0/P_0. As shown in this figure, the proposed approximation model reproduces well the distribution parameter numerical results in the subcooled boiling region.

3.4.2.2. Edge subchannel. The variation of the coefficients a and b in Equation (37) relative to D_0/P_0 can be approximated by the following equation, which reproduces the results of the numerical analysis. Here, the ratio of the distance between the rod and the channel wall and the gap width between rods, k, is set to $k = 1.0$.

$$a = 77.83\exp\{-3.781(D_0/P_0)\} + 26.30, \\ b = 0.8202 \quad (43)$$

The distribution parameters can be obtained using Equation (35) which is the distribution parameter for bulk boiling region and using Equations (37) and (43) to approximate the numerical calculation conveniently for any D_0/P_0 ranging from 0.2 to 0.9. Figure 9(b) compares the distribution parameter calculated using Equations (35), (37) and (43) for a typical D_0/P_0 with the analytical values. As shown in this figure, the proposed approximation model reproduces well the results of the numerical calculation of the distribution parameter in the subcooled boiling region. As shown in Figure 9(b), although the proposed model was derived assuming $k = 1$, it can be confirmed that the sensitivity of k to the distribution parameter is small, and the derived proposed model is applicable in the range of $0.9 \le k \le 2.0$.

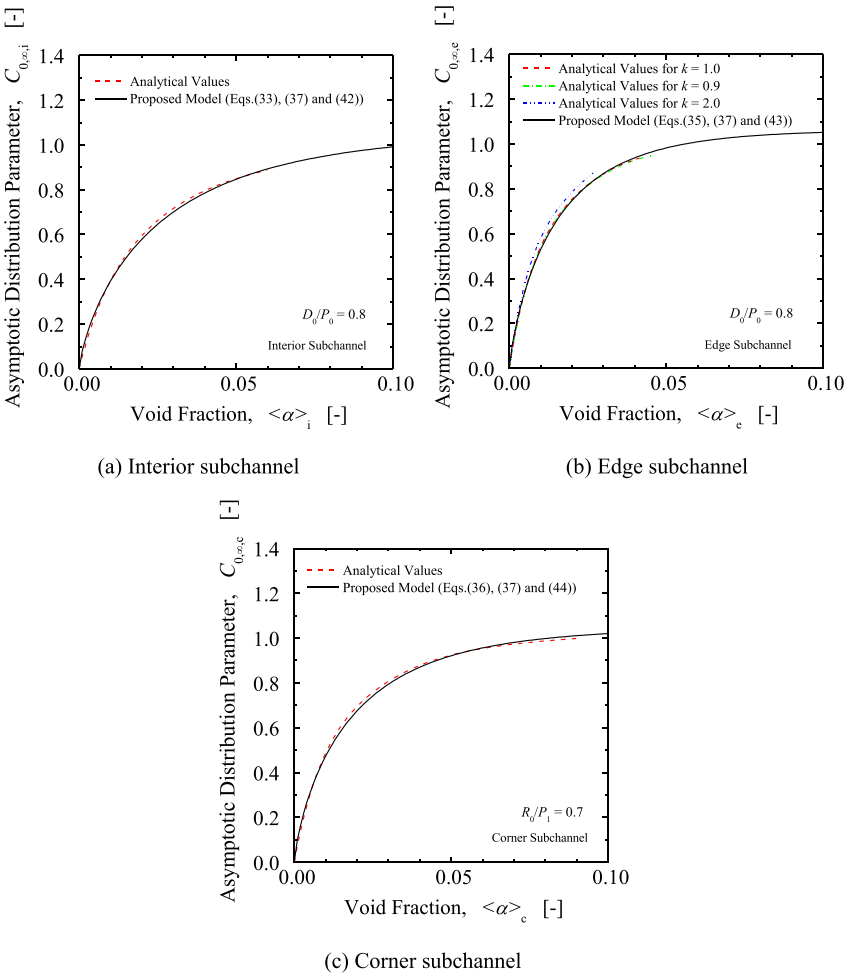

(a) Interior subchannel

(b) Edge subchannel

(c) Corner subchannel

Figure 9. Comparison between analytically calculated distribution parameters and proposed model for (a) interior subchannel, (b) edge subchannel, and (c) corner subchannel.

Table 2. Distribution parameter models for each subchannel type.

	Interior	Corner	Edge
C_∞ correlation	$C_\infty = 0.9999 + 0.1717\left(\frac{D_0}{P_0}\right) - 0.2215\left(\frac{D_0}{P_0}\right)^2 + 0.1263\left(\frac{D_0}{P_0}\right)^3$	$C_\infty = 1.016 + 0.09392\left(\frac{R_0}{P_1}\right) - 0.1606\left(\frac{R_0}{P_1}\right)^2 + 0.1304\left(\frac{R_0}{P_1}\right)^3$	$C_\infty = 1.036 + 0.07044\left(\frac{D_0}{P_0}\right) - 0.08637\left(\frac{D_0}{P_0}\right)^2 + 0.05053\left(\frac{D_0}{P_0}\right)^3$
C_0 correlation	$C_0 = \left(C_\infty - (C_\infty - 1)\sqrt{\frac{\rho_g}{\rho_f}}\right)\left(1 - e^{-aa^b}\right)$		
Coefficient a	$a = 24.87\exp\left\{-3.686\left(\frac{D_0}{P_0}\right)\right\} + 14.95$	$a = 52.12\exp\left\{-2.044\left(\frac{R_0}{P_1}\right)\right\} + 9.564$	$a = 77.83\exp\left\{-3.781\left(\frac{D_0}{P_0}\right)\right\} + 26.30$
Coefficient b	$b = 0.7731$	$b = 0.7821$	$b = 0.8202$
Applicable range	$0.2 \le \frac{D_0}{P_0} \le 0.9$	$0.2 \le \frac{R_0}{P_1} \le 0.8$	$0.2 \le \frac{D_0}{P_0} \le 0.9$ $0.9 \le k \le 2$

Table 3. Distribution parameters of the proposed model for the representative BWR fuel bundles .

Bundle design	Interior	Corner	Edge
8 × 8 (NUPEC)	1.058	1.044	1.062
9 × 9 (Type-A)	1.059	1.043	1.062
9 × 9 (Type-B)	1.058	1.043	1.062
10 × 10 (GE14)	1.060	1.042	1.063

3.4.2.3. Corner subchannel. The variation of the coefficients a and b in Equation (37) relative to R_0/P_1 can be approximated as an equation that reproduces the results of the numerical analysis as follows.

$$a = 52.12\exp\{-2.044(R_0/P_1)\} + 9.564$$
$$b = 0.7821. \quad (44)$$

The distribution parameter can be obtained using Equation (36) which is the distribution parameter for the bulk boiling region and using Equations (37) and (44) to approximate the numerical calculation conveniently for any R_0/P_1 ranging from 0.2 to 0.8. Figure 9(c) compares the distribution parameter calculated using Equations (36), (37), and (44) for a typical R_0/P_1 with the analytical values. As shown in this figure, the proposed approximation model reproduces well the results of the numerical calculation of the distribution parameter in the subcooled boiling region.

The distribution parameter models for each subchannel type are summarized in Table 2. The distribution parameters of each subchannel type for the representative BWR fuel bundles of Table 1 are in Table 3.

4. Evaluation of modeled distribution parameters in subchannels

This section discusses the evaluation of the distribution parameter models for each subchannel type presented in Section 3. The semi-experimental data of the distribution parameter for each subchannel are obtained from measured local void fraction data for each subchannel collected in the NUPEC rod bundle test and assumed mixture volumetric flux distribution in each subchannel. The distribution parameter model is compared with the semi-experimental data.

4.1. Interior subchannel

The interior subchannels of the 8 × 8 fuel simulator used in the NUPEC test are $D_0/P_0 = 0.759$. The mixture volumetric flux distribution in Equation (12) is assumed for all the interior subchannels, and the distribution parameter is calculated together with the measured local void fraction. Figure 10 compares the measured distribution parameters with those calculated using Equations (33), (37), and (42).

The mean absolute error, m_d, standard deviation, s_d, mean relative deviation, m_{rel}, and mean absolute relative deviation, $m_{rel,ab}$, of calculated and measured distribution parameter values are 0.00495, 0.0102, 0.480%, and 0.867%, respectively. Definitions of these statistical parameters are given as follows.

$$m_d = \frac{1}{N}\sum_{j=1}^{N}\left(C_{0,\mathrm{cal}} - C_{0,\mathrm{exp}}\right)_j, \quad (45)$$

$$s_d = \sqrt{\frac{1}{N-1}\sum_{j=1}^{N}\left\{\left(C_{0,\mathrm{cal}} - C_{0,\mathrm{exp}}\right)_j - m_d\right\}^2}, \quad (46)$$

$$m_{rel} = \frac{1}{N}\sum_{j=1}^{N}\left(\frac{C_{0,\mathrm{cal}} - C_{0,\mathrm{exp}}}{C_{0,\mathrm{exp}}}\right)_j, \quad (47)$$

$$m_{rel,ab} = \frac{1}{N}\sum_{j=1}^{N}\left(\frac{\left|C_{0,\mathrm{cal}} - C_{0,\mathrm{exp}}\right|}{C_{0,\mathrm{exp}}}\right)_j. \quad (48)$$

The distribution parameter model developed in this study is derived by assuming the void fraction and mixture volumetric flux distributions in the subchannel. The model does not include any parameters for adjustment with the experimental data. The developed

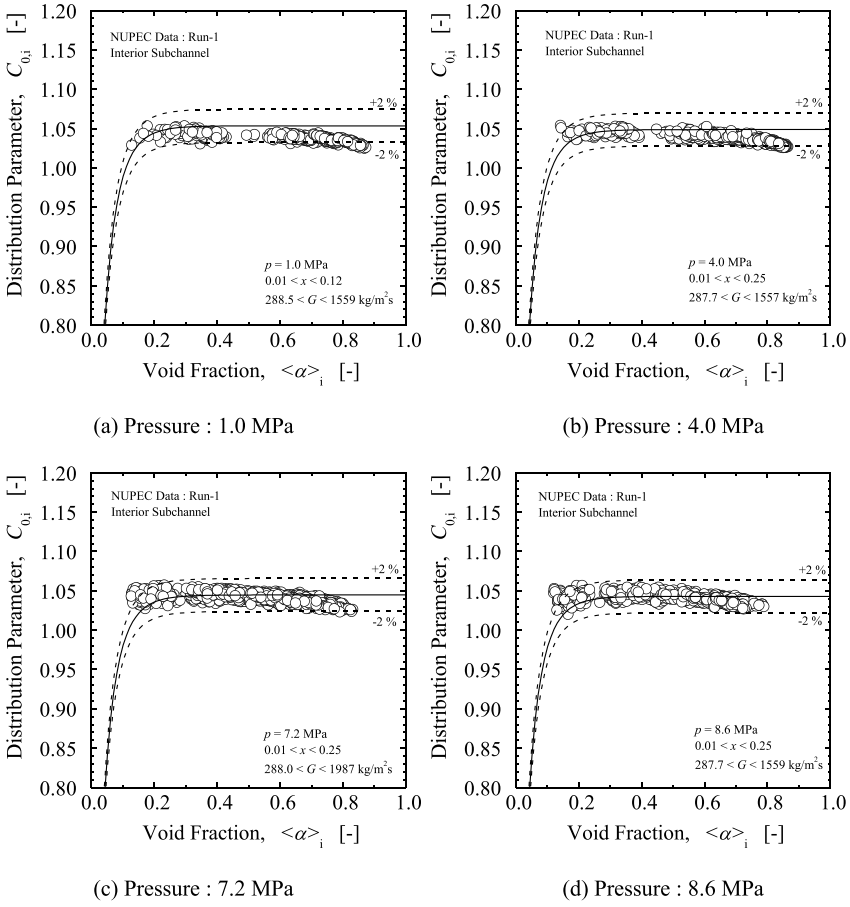

(a) Pressure : 1.0 MPa

(b) Pressure : 4.0 MPa

(c) Pressure : 7.2 MPa

(d) Pressure : 8.6 MPa

Figure 10. Applicability of proposed distribution parameter model to the semi-experimental data of interior subchannels in NUPEC test.

model reproduces the actual phenomena better than the conventional model, which assumes the distribution parameter to be unity, for the experimental data with the geometry of an actual fuel bundle and the prototypic BWR thermal-hydraulic conditions. Therefore, the applicability of the developed model to the actual fuel bundle is indicated. It should be noted here that the prediction accuracy deteriorates when the flow regime transition from dispersed to separated two-phase flows occurs. The experimental distribution parameter gradually decreases toward unity as the subchannel average void fraction approaches unity.

The measured value of the distribution parameter in the bulk boiling region under high-temperature and high-pressure conditions is confirmed to be about 5% larger than unity, currently used in codes. In most subchannel analysis codes, the distribution parameter is hypothetically set to unity. Therefore, the calculated void fraction in the subchannel analysis code is overestimated due to underestimated distribution parameter. By incorporating the proposed model into the subchannel analysis code, the effect of the void fraction distribution in the subchannel can be considered. The overestimation of the calculated value is expected to be mitigated.

4.2. Edge subchannel

As in the case of the interior subchannel, the mixture volumetric flux distribution of Equation (21) is assumed for each of the edge subchannels of the 8 × 8 fuel simulator used in the NUPEC test. Figure 11 compares these measured distribution parameters with those calculated using Equations (35), (37), and (43). The mean absolute error, m_d, standard deviation, s_d, mean relative deviation, m_{rel}, and mean absolute relative deviation, $m_{rel,ab}$, of the calculated and measured distribution parameter values are 0.0161, 0.0113, 1.57%, and 1.65%, respectively. The developed model reproduces the actual distribution parameter better than the conventional model assuming the distribution constant to be unity. As in the case of the interior subchannel, the measured value of the distribution parameter is shown to be larger than unity in the bulk boiling region, which is assumed in many subchannel analysis codes.

4.3. Corner subchannel

The corner subchannels of the 8 × 8 fuel simulator used in the NUPEC test are $R_0/P_1 = 0.631$. The mixture volumetric flux distribution in Equation (30) is assumed for each of the four corner

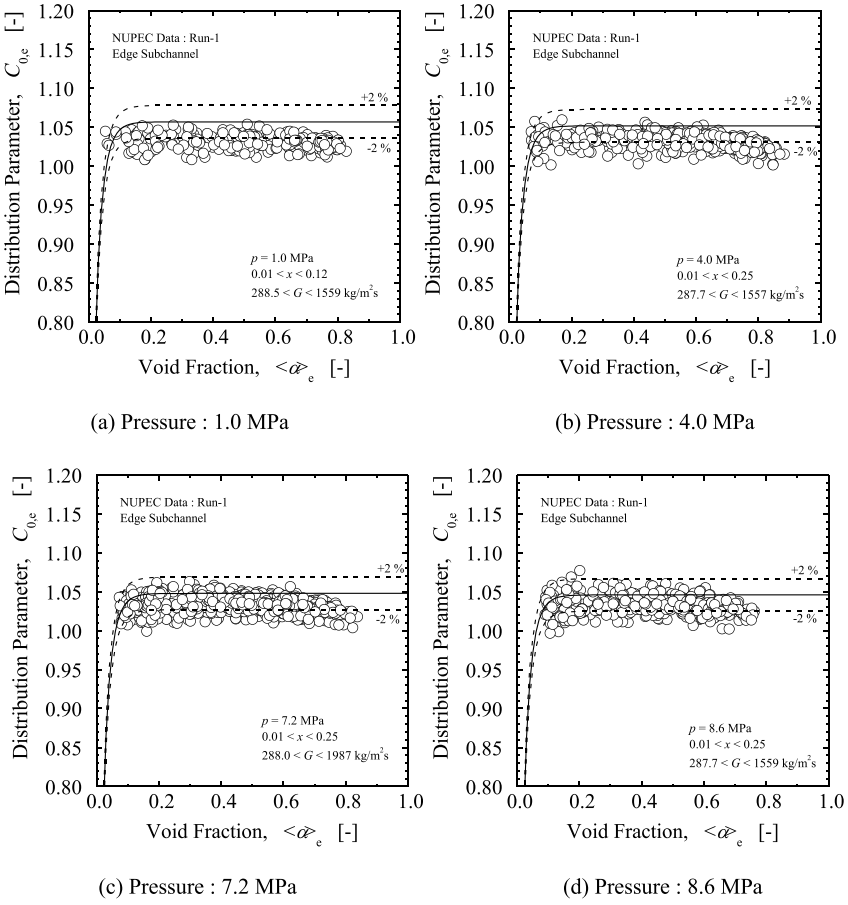

Figure 11. Applicability of proposed distribution parameter model to the semi-experimental data of edge subchannels in NUPEC test.

subchannels, and the distribution parameter can be calculated together with the measured local void fraction. Figure 12 compares the measured distribution parameters with those calculated using Equations (36), (37), and (44). The mean absolute error, m_d, standard deviation, s_d, mean relative deviation, m_{rel}, and mean absolute relative deviation, $m_{rel,ab}$, of the calculated and measured distribution parameter values are −0.00487, 0.00949, −0.469%, and 0.619%, respectively. The developed model reproduces the actual distribution parameter better than the conventional model assuming the distribution parameter of unity. Therefore, the applicability of the developed model to actual fuel bundles is indicated.

As in the case of the interior subchannel and edge subchannel, it is shown that the measured value of the distribution parameter is larger than unity in the bulk boiling region, which is assumed by many subchannel analysis codes. Finally, for any subchannel type, it is clear that the current subchannel analysis codes underestimate the distribution parameter. The current subchannel analysis codes have the tendency to overestimate the void fraction even for the cross-sectional average void fraction of the whole bundle.

5. Effect of distribution parameter modeling on subchannel code analysis

The effect of distribution parameter modeling on the subchannel analysis is investigated. Here, the NASCA code, which has been developed for the analysis of two-phase flow behavior in a BWR fuel bundle, is used.

The NASCA code is a three-fluid field subchannel code that treats gas, liquid film, and droplet as fluid fields. The momentum transfer term between the gas and liquid phases has a large influence on the void fraction calculation results. The momentum transfer term is expressed by considering the interfacial drag force in the conservation equations and expressed by Equations (1) and (2) in the NASCA code. However, in the NASCA code, C_0 in Equation (2) is assumed to be unity regardless of the subchannel type. As shown in Section 4, the distribution parameter in the bulk boiling region takes a value greater than unity at the subchannel scale. It is expected to impact the predicted value of the void fraction when the developed distribution parameter model for each subchannel type is implemented into the NASCA code. The only difference between the original and modified NASCA codes is the distribution parameter value. It should be noted here that other constitutive equations as the void drift model, turbulent mixing model, and so on, are optimized under the assumed distribution

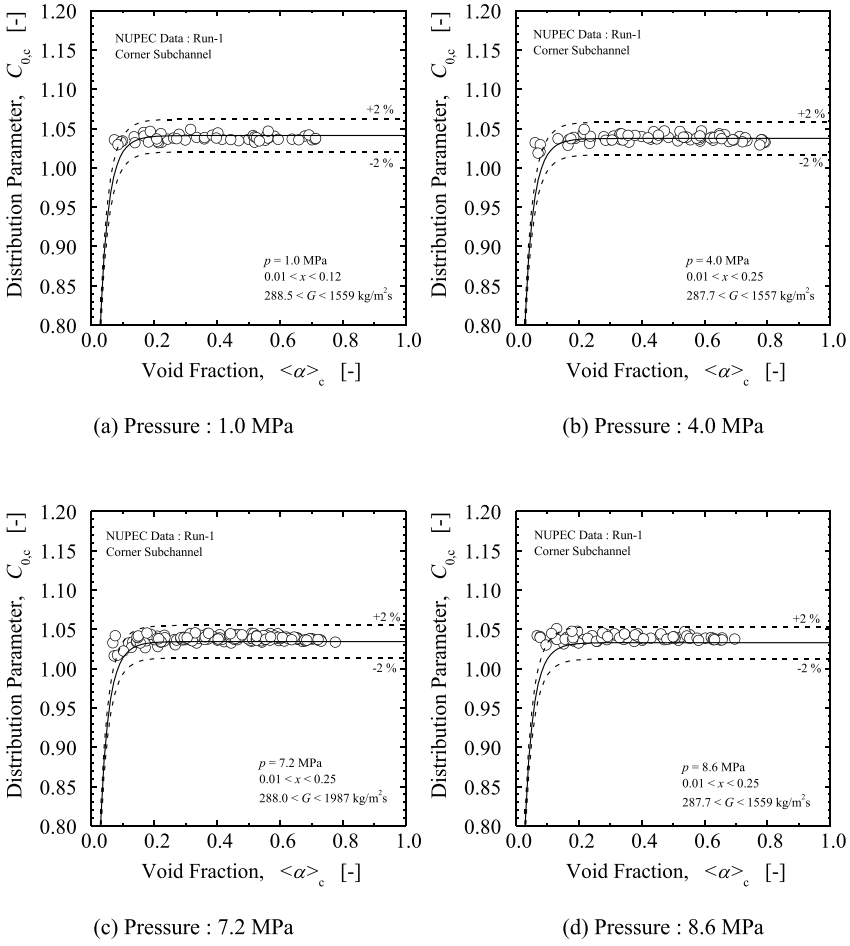

Figure 12. Applicability of proposed distribution parameter model to the semi-experimental data of corner subchannels in NUPEC test.

parameter being unity. A comparison between the original and modified NASCA codes can show the effect of the subchannel distribution parameter on the code predictions. As mentioned above, the distribution parameter model for each subchannel type in the bundle is developed, which is expected to improve the prediction accuracy of the void fraction by incorporating it into the NASCA code.

For the NUPEC rod bundle void fraction test data presented in Section 2, the calculated cross-sectional average void fraction of the whole bundle for the original and modified NASCA codes are compared with the measured data to understand the global effect of the subchannel distribution parameter on the cross-sectional average void fraction. The results are shown in Figure 13. Table 4 shows the results of

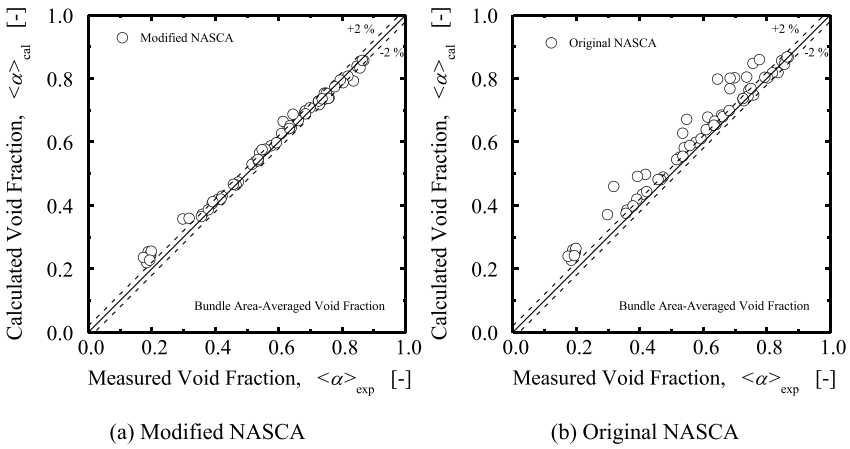

Figure 13. Comparisons of measured and calculated area-averaged void fraction for (a) modified NASCA(implemented proposed distribution parameter model) and (b) original NASCA.

Table 4. Comparisons of prediction performance for void fraction between original and modified NASCA.

Evaluation item	Original NASCA	Modified NASCA
Mean absolute error, m_d	0.0382	0.0112
Standard deviation, s_d	0.0385	0.0217
Mean relative deviation, m_{rel}	9.49%	4.37%
Mean absolute relative deviation, $m_{rel,ab}$	9.67%	5.14%

Table 5. Comparisons of prediction performance for distribution parameter between the proposed model and NUPEC data.

Evaluation item	Interior Subchannel	Edge Subchannel	Corner Subchannel
Mean absolute error, m_d	0.00495	0.0161	−0.00487
Standard deviation, s_d	0.0102	0.0113	0.00949
Mean relative deviation, m_{rel}	0.480%	1.57%	−0.469%
Mean absolute relative deviation, $m_{rel,ab}$	0.867%	1.65%	0.619%

the evaluation made by replacing the distribution parameter with the void fraction in each of Equations (45) to (48) to derive the comparison indices between the experimental and calculated values. Figure 13 and Table 4 indicate that the values of the subchannel distribution parameter impact the void fraction prediction. The cross-sectional average void fraction calculated by the original NASCA overestimates the measured value by about 4% in the mean absolute deviation and about 9% in the mean relative deviation. This may be because the distribution parameters of the subchannels are larger than unity, and the original NASCA cannot consider the effect of these distribution parameter values. The deviation of the void fraction from the measured value appears as the deviation of the average density of the moderator, which is important in the neutron behavior in a core, so it is critical to reduce the deviation as much as possible.

6. Conclusions

In this study, distribution parameter models of subchannel flow paths in a fuel bundle were proposed for the inner subchannel, edge subchannel, and corner subchannel. By formulating the distribution parameter of the subchannel, it could be enabled to accurately simulate the distributions of subchannel area-average void fraction and mixture volumetric flux by the subchannel analysis code.

The distribution parameter model was derived by assuming the void fraction and mixture volumetric flux distributions, and no empirical parameters were used to adjust the experimental data. The applicability of the model was indicated by using the NUPEC rod bundle void fraction test data, in which the void fraction of each subchannel was measured under high-temperature and high-pressure conditions, including those of the prototypic BWR. The fuel bundle simulator, whose design was the same as that of fuel bundles loaded in BWRs, was used for the NUPEC test. The void fraction was measured as a local distribution using the X-ray CT, and the distribution parameter was evaluated in combination with the assumed mixture volumetric flux.

The distribution parameters evaluated based on the experimental data were compared with those calculated from the proposed model. The proposed model showed excellent predictive performances for the distribution parameters based on experimental values for each subchannel type. The statistical values of the predictive performances are summarized in Table 5. The developed model reproduced the actual distribution parameter better than the conventional assumption, which assumes the distribution parameter to be unity, for the experimental data with the geometry of the prototypic fuel bundle and thermal-hydraulic conditions. Therefore, the applicability of the developed model to the actual fuel bundle was indicated.

To show the effect of the subchannel distribution parameter on the subchannel analysis code predictions, the developed distribution parameter model for each subchannel was implemented in the subchannel analysis code NASCA. The improved NASCA code was compared with the NUPEC rod bundle void fraction test data. The comparison results for the original NASCA code, absolute error, m_d, standard deviation, s_d, mean relative deviation, m_{rel}, and mean absolute relative deviation, $m_{rel,ab}$, of calculated and measured area-averaged void fraction values were 0.0382, 0.0385, 9.49%, and 9.67%, respectively. The original NASCA code assumes a distribution parameter of unity, and in the present study, it overestimated the cross-sectional area-averaged void fraction by about 4% in the mean absolute deviation and by about 9% in the mean relative deviation. The NASCA code that implemented the proposed model showed improved prediction performance, and the mean absolute error, m_d, standard deviation, s_d, mean relative deviation, m_{rel}, and mean absolute relative deviation, $m_{rel,ab}$, of calculated and measured area-averaged void fraction values were 0.0112, 0.0217, 4.37%, and 5.14%, respectively. The applicability of the developed distribution parameter model was

indicated for the cross-sectional average void fraction of the whole prototypic BWR fuel bundle collected under uniform power distribution. The applicable BWR rod design of the developed model is summarized in Table 2.

A future study should address the effects of several factors on the distribution parameter. They are (a) fuel rod power distribution, (b) grid spacers, and (c) enthalpy gradient due to unheated rods. Although insignificant effects of the fuel rod power distribution and enthalpy gradient due to unheated rods on the bundle average distribution parameter were reported [25], the effects on the subchannel average distribution parameter were not experimentally examined. It was reported that the effect of the spacer grid on the bundle average void fraction was diminished within a short distance from the space grid [26]. However, the effect of the spacer grid on the subchannel average distribution parameter was not experimentally examined.

The lateral force models implemented in the subchannel analysis code, void drift model and turbulent mixing model, are optimized for the distribution parameter being unity. When the developed distribution parameter model is applied to simulate the distributions of void fraction and flow velocity, the optimization of the lateral force models should be revisited. The developed distribution parameter model is expected to improve the modeling accuracy of the interfacial drag force. To further enhance the modeling accuracy of the interfacial drag force, the void fraction covariance and relative velocity covariance models should be modeled in a future study [27]. The reproducibility of the moderator density is important in neutron behavior in a core. The reliability of the core simulation is expected to be improved by applying the developed model.

Nomenclature

a	coefficient
A_c	flow area
A_{wp}	bubble layer area
a_i	interfacial area concentration
b	exponent
C_0	distribution parameter
C_D	drag coefficient
D_0	rod diameter
j	mixture volumetric flux
$j_{c,p}$	maximum mixture volumetric flux in a given radial direction of p-type subchannel
$j_{c0,p}$	maximum mixture volumetric flux within a p-type subchannel
k	ratio of the gap between the rod and channel wall to the gap between rods
M_{if}	interfacial drag force acting on liquid phase
M_{ig}	interfacial drag force acting on gas phase
m_d	mean absolute error
m_j	exponent for volumetric flux distribution
m_{rel}	mean relative deviation
$m_{rel,ab}$	mean absolute relative deviation
m_α	exponent for void fraction distribution
P_0	rod pitch
P_1	distance from rod center to the wall of the flow channel
R_0	rod radius
R_c	distance from the origin to the position where $j = j_c$
R_p	radius of round tube
r	radial position from rod surface
s_d	standard deviation
v_r	relative velocity between gas and liquid phase
x_{wp}	bubble layer thickness
Greek symbols	
α	void fraction
$\alpha_{c0,p}$	void fraction at the center of a p-type subchannel
α_{wp}	void fraction at assumed square bubble layer
Λ	the ratio of the subchannel distribution parameter to round tube distribution parameter
ψ	shape factor
θ	azimuthal position
θ_0	threshold angle for edge subchannel
θ'	angle where the maximum value of mixture volumetric flux occurs
ρ	density
Subscripts	
c	corner subchannel
cal	calculated value
e	edge subchannel
exp	measured value
f	liquid phase
g	gas phase
i	interior subchannel
p	subchannel type
rt	round tube
∞	asymptotic value

Acknowledgments

One of the authors (T. Hibiki) appreciates the support provided by the City University of Hong Kong (Project Number: 7005924).

Disclosure statement

No potential conflict of interest was reported by the author(s).

References

[1] Masumi R, Iwata Y, Yoshimori H. Initial core design and start-up experience of Shika 2. Proceedings of 2006 Spring Meeting of the Atomic Energy Society of Japan, Oarai, Ibaraki, Japan. 2006. p. 292.

[2] Tada K, Fujita T, Endo T, et al. Application of quick subchannel analysis method for three-dimensional pin-by-pin BWR core calculations. J Nucl Sci

Technol. 2011;48(12):1437–1452. doi: 10.1080/18811248.2011.9711837
[3] Yeoh GH. Thermal hydraulic considerations of nuclear reactor systems: Past, present and future challenges. Exp Comput Multiph Flow. 2019;1(1):3–27. doi: 10.1007/s42757-019-0002-5
[4] Chuang TJ, Hibiki T. Vertical upward two-phase flow CFD using interfacial area transport equation. Prog Nucl Ener. 2015;85:415–427. Elsevier Ltd. doi: 10.1016/j.pnucene.2015.07.008
[5] Wheeler CL, Stewart CW, Cena RJ, et al. COBRA-IV-I: an interim version of COBRA for thermal-hydraulic analysis of rod bundle nuclear fuel elements and cores. Richland, WA (United States): Pacific Northwest Laboratory; 1976.
[6] Thurgood JM COBRA/TRAC-A thermal-hydraulic code for transient analysis of nuclear reactor vessels and primary coolant systems. Pacific Northwest Lab, Report [Internet]. 1983 [cited NUREG/CR 2021 Jul 19]; -3046. Available from: http://ci.nii.ac.jp/naid/10003633162/ja/.
[7] Salko JR, Avramova M, Wysocki A, et al. CTF 4.0 theory manual. Oak Ridge, TN (United States): Oak Ridge National Laboratory; 2019.
[8] Sugawara S. Analytical prediction of CHF by FIDAS code based on three-fluid and film-dryout model. J Nucl Sci Technol. 1990;27(1):12–29. doi: 10.1080/18811248.1990.9731148
[9] Kitou K, Nishida K, Ishii Y, et al. Subchannel analysis to investigate the fuel assembly for the supercritical-water-cooled power reactor. J Nucl Sci Technol. 2004;41(11):1075–1082. doi: 10.1080/18811248.2004.9726332
[10] Hotta A, Zhang M, Shirai H. Application of TRAC/BF1-ENTRÉE-NASCA to OECD NEA/NSC BWR turbine trip benchmark. Nucl Sci Eng. 2004;148(2):208–225. doi: 10.13182/NSE04-A2452
[11] Ishii M, Hibiki T. Thermo-fluid dynamics of two-phase flow. New York, NY: Springer New York; 2011.
[12] Enrique Julia J, Hibiki T, Ishii M, et al. Drift-flux model in a sub-channel of rod bundle geometry. Intern J Heat Mass Trans. 2009;52(13–14):3032–3041. doi: 10.1016/j.ijheatmasstransfer.2009.02.012
[13] Utsuno H, Hochreiter L, Kasahara F, et al. NUPEC BWR Full-size Fine-mesh Bundle Test (BFBT) Benchmark. 2006.
[14] Nuclear Power Engineering Test Center. Report on proving test on reliability for BWR fuel bundles (void fraction tests in BWR fuel bundles - support document). Tokyo; 1992.
[15] Nuclear Power Engineering Corporation. Report on proving test on reliability for BWR fuel bundles (supplement) (void fraction tests for high burnup fuel bundle - overall evaluation). Tokyo; 1993.
[16] Inoue A, Kurosu T, Aoki T, et al. Void fraction distribution in bwr fuel assembly and evaluation of subchannel code. J Nucl Sci Technol. 1995;32(7):629–640. doi: 10.1080/18811248.1995.9731754
[17] Ishii M, Mishima K. Two-fluid model and hydrodynamic constitutive relations. Nucl Eng Des. 1984;82(2–3):107–126. doi: 10.1016/0029-5493(84)90207-3
[18] Hibiki T, Situ R, Mi Y, et al. Modeling of bubble-layer thickness for formulation of one-dimensional interfacial area transport equation in subcooled boiling two-phase flow. Inter J Heat Mass Trans. 2003;46:1409–1423. doi: 10.1016/S0017-9310(02)00418-0 InternetAvailable from: www.elsevier.com/locate/ijhmt. 8.
[19] Ishii M. One-dimensional drift-flux model and constitutive equations for relative motion between phases in various two-phase flow regimes. Illinois (USA): Argonne National Laboratory; 1977.
[20] Ozaki T, Hibiki T. Modeling of sub-channel scale distribution parameter and its validation based on database of rod bundle void fraction measurement test under prototypic BWR Conditions. Jpn J Multiphase Flow. 2021;35(550):543 .
[21] Yun B-J, Park G-C, Julia EJ, et al. Flow structure of subcooled boiling water flow in a subchannel of 3 × 3 rod bundles. J Nucl Sci Technol. 2008;45(5):402–422. doi: 10.1080/18811248.2008.9711450
[22] Inoue A, Kurosu T, Aoki T, et al. Void measurement of BWR fuel assembly. J Atom Ener Soc Jpn / Atom Ener Society Jpn. 1995;37(8):710–720. doi: 10.3327/jaesj.37.710 InternetAvailable from: http://www.jstage.jst.go.jp/article/jaesj1959/37/8/37_8_710/_article/-char/ja/
[23] Peakman A, Grove C, Fitzgerald K, et al. Development of an equilibrium loading pattern and whole-core fuel performance assessment in the Advanced Boiling Water Reactor (ABWR) with UO2 and U3Si2 fuels. Prog Nucl Energy. 2019;117:117. doi:10.1016/j.pnucene.2019.103053
[24] Tsukuda Y, Hayashi H, Kamikura K, et al. Proving test on thermal-hydraulic performance of BWR fuel assemblies. Trans Atom Ener Soc Jpn. 2002;1(4):384–403. InternetAvailable from: https://www.jstage.jst.go.jp/article/taesj2002/1/4/1_4_384/_article
[25] Ozaki T, Suzuki R, Mashiko H, et al. Development of drift-flux model based on 8×8 BWR rod bundle geometry experiments under prototypic temperature and pressure conditions. J Nucl Sci Technol. 2013;50(6):563–580. doi: 10.1080/00223131.2013.785277
[26] Yang X, Schlegel JP, Liu Y, et al. Measurement and modeling of two-phase flow parameters in scaled 8×8 BWR rod bundle. Int J Heat Fluid Flow. 2012;34:85–97. doi:10.1016/j.ijheatfluidflow.2012.02.001
[27] Ozaki T, Hibiki T. Modeling of distribution parameter, void fraction covariance and relative velocity covariance for upward steam-water boiling flow in rod bundle. J Nucl Sci Technol. 2017;55(4):386–399. doi: 10.1080/00223131.2017.1403382